Cytokinesis from nanometers to micrometers and microseconds to minutes

P. Kothari, E.S. Schiffhauer, D.N. Robinson[1]
Johns Hopkins University, Baltimore, MD, United States
[1]*Corresponding author: E-mail: dnr@jhmi.edu*

CHAPTER OUTLINE

Methods in Cell Biology, Volume 137, ISSN 0091-679X, http://dx.doi.org/10.1016/bs.mcb.2016.03.038

Abstract

Cytokinesis, a model cell shape change event, is controlled by an integrated system that coordinates the mitotic spindle signals with a mechanoresponsive cytoskeletal network that drives contractility and furrow ingression. Quantitative methods that measure cell mechanics, mechanoresponse (mechanical stress-induced protein accumulation), protein dynamics, and molecular interactions are necessary to provide insight into both the mechanical and biochemical components involved in cytokinesis and cell shape regulation. Micropipette aspiration, fluorescence correlation and cross-correlation spectroscopy, and fluorescence recovery after photobleaching are valuable methods for measuring cell mechanics and protein dynamics in vivo that occur on nanometer to micron length-scales, and microsecond to minute timescales. Collectively, these methods provide the ability to quantify the molecular interactions that control the cell's ability to change shape and undergo cytokinesis.

INTRODUCTION

Cytokinesis is a mechanical and biochemical process, studied since the development of the first microscopes. Because of the dramatic nature of the cell shape change, the condensation of chromosomes, their movement along microtubules, and the pinching of the membrane, the process of cell division has garnered attention from the very earliest phases of cell biology. It was not until the 1940s when Crick recognized that the cytoplasm is thixotropic (viscoelastic) in nature (Crick & Hughes, 1950). This realization facilitated researchers, including Rappaport and Hiramoto, to appreciate that cytokinesis is a force-generating process (Hiramoto, 1963; Rappaport, 1967). The resulting, profound implication is that chemical signaling pathways do not act in isolation to promote furrow contraction; the cytokinetic machinery also requires a mechanosensory and mechanotransducer (Effler, Iglesias, & Robinson, 2007; Srivastava, Iglesias, & Robinson, 2015). In fact, Newton's third law dictates that the force-generating machinery must be both sensitive and responsive to the resulting resistive stresses. Such stresses impact the assembly, contraction, remodeling, and ultimately completion of cytokinesis. Although the field has identified many of the components involved in cytokinesis, much remains to be uncovered about how these components assemble and how their dynamics impact furrow ingression. Describing this network of cytoskeletal and signaling proteins is key to understanding how the cytokinetic machine is built, tuned, and maintained under different environmental stresses and in various genetic backgrounds. Furthermore, cytokinesis is an ideal model process for understanding the general fundamental principles of cell shape change events, including contractility, adhesion, and the effect of Laplace pressures. Thus, studying this single process can help unravel the mechanisms behind cell shape changes in other systems and higher order structures.

Although transillumination microscopy has provided us with a wealth of information regarding dividing cells, this approach fails to capture the spatial and

temporal details of this complex mechanical process. The purpose of this review is to describe valuable quantitative techniques that are currently being used to study cytokinesis at the molecular level. While cytokinesis occurs over the timescale of minutes, the process is driven by associations, interactions, and forces that occur on a millisecond-to-second timescale. During cytokinesis, the cell's ability to respond to various external perturbations is dependent upon transient and dynamic interactions that allow for rapid molecular-level responses. Studying these molecular interactions using high spatial and temporal resolution is critical for developing a thorough understanding of the underlying molecular interactions driving cytokinesis. The methods described here are applicable to single-cell systems, and have been used with the social amoeba *Dictyostelium discoideum* (Kee et al., 2012; Srivastava & Robinson, 2015), *Drosophila melanogaster* S2 cells (Kim et al., 2015), as well as mammalian cells (Schiffhauer et al., 2016; Sun et al., 2014).

1. MICROPIPETTE ASPIRATION

1.1 OVERVIEW

During cytokinesis, the division machinery both generates and responds to evolving force vectors in the cell cortex. Therefore, it is essential to observe the cellular response to imposed forces in the physiological range. Methods for applying forces to cells include atomic force microscopy (Matzke, Jacobson, & Radmacher, 2001), optical traps (Ashkin, Dziedzic, & Yamane, 1987), magnetic beads (Mijailovich, Kojic, Zivkovic, Fabry, & Fredberg, 2002), global cell compression (Kee et al., 2012; Srivastava & Robinson, 2015), and real-time deformability cytometry (RT-DC) (Otto et al., 2015). Although each of these techniques has been useful for addressing specific questions about biochemical and mechanical properties of cells, they often probe smaller or larger force and spatial regimes, with variable accuracy for quantifying the magnitude, direction, and spatial distribution of the force imposed. Micropipette aspiration (MPA) is a powerful system for applying localized forces in the nanoNewton (nN) range to individual cells, closely mimicking the localized forces cells generated and experienced at the cleavage furrow (Gerald, Dai, Ting-Beall, & De Lozanne, 1998; Hiramoto, 1963, 1990; Hochmuth, 2000; Rappaport, 1967; Reichl et al., 2008; Wolpert, 1966; Zhang & Robinson, 2005).

MPA can be used for two major purposes: (1) to measure the intrinsic mechanical properties of cells and (2) to study the accumulation of elements of the cytokinetic machinery in response to applied force, separating force-dependent protein behavior from chemical signals emanating from the mitotic spindle in mitosis.

1.2 CELL MECHANICS

To measure the intrinsic properties of cells, one must consider the cell as a viscoelastic material with both viscous and elastic components. The mechanical

properties of a cell in suspension are largely dominated by the cortical cytoskeleton with some contribution from the cytoplasm. Less than 5% of the cell's elasticity is borne by the plasma membrane (Luo, Srivastava, Ren, & Robinson, 2014). If aspirated upon by a fixed pressure into a pipette with radius R_p, a cell will deform into the pipette (length into pipette, L_p, Fig. 1A), until tension in the cortex of the cell, T_c, opposes the force applied. If the cell were perfectly elastic, it would immediately extend to this distance and go no further. By measuring L_p over time on a cell, one can observe that a cell gradually extends into the pipette before stabilizing,

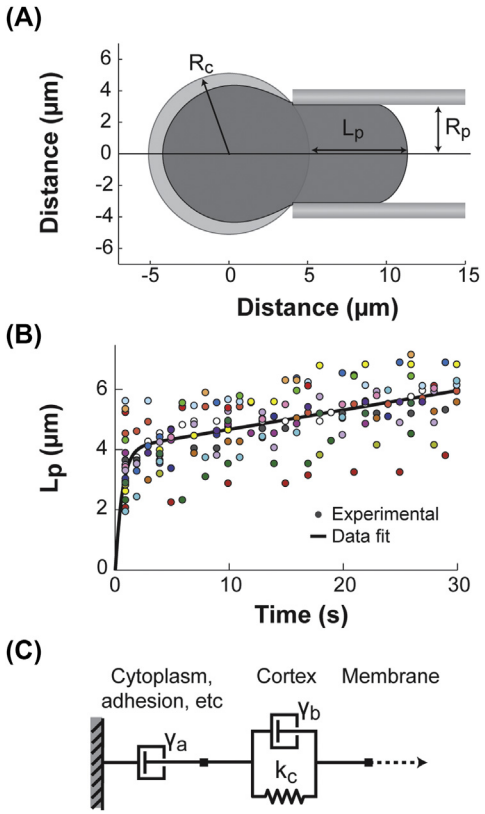

FIGURE 1 Micropipette aspiration to measure cell mechanics.

(A) A schematic of measurements made on a cell aspirated into a pipette where L_p is the distance the cell deforms into the pipette, R_p is the radius of the pipette, and R_c is the radius of the cell. (B) A measurement of a number of *Dictyostelium* cells deforming into the pipette over time. (C) Model of cell mechanics, where γ_b is determined by the initial rate of deformation, γ_a is determined by the slope of the second flow, and k_c defines the elastic component of the cell cortex.

Adapted from Yang, L., Effler, J. C., Kutscher, B. L., Sullivan, S. P., Robinson, D. N., & Iglesias, P. A. (2008). Modeling cellular deformations using the level set formalism. Biomedcentral Systems Biology, 2, *68–84.*

and at pressures greater than critical pressure, P_c, (see later discussion), the cell continues to flow into the pipette slowly (Fig. 1B). The slope of these two phases is determined by the cell's viscous component. We can describe then, the mechanics of a cell using the diagram in Fig. 1C, where the slope of the initial deformation phase is determined by the parallel damper, γ_b, and the slope of the second flow phase, by the damper in series, γ_a (Yang et al., 2008).

A common method for comparing the elasticity of two cells, or of a cell in different phases of the cell cycle, is the measurement of cortical tension (T_c). To get an accurate reading of tension, one must determine the pressure at which the cell is deformed to $L_p = R_p$, or the critical pressure, P_c. It is essential to allow sufficient time for the full relaxation of the parallel damper and to not apply so much pressure as to enter the regime of the damper in series. Then, Eq. (1) can be used to determine T_c:

$$\Delta P_c = 2T_c\left(\frac{1}{R_p} - \frac{1}{R_c}\right) \tag{1}$$

where P_c is the critical pressure, T_c is the cortical tension, R_p is the radius of the pipette, and R_c is the radius of the cell.

1.3 PROTEIN MECHANOACCUMULATION

Similar to using MPA to study cell mechanics, MPA can be used to study the mechanoresponsiveness or accumulation of proteins in response to mechanical stress (force/area). However, the pressure imposed varies by cell type and ranges from 0.5 to 3 nN/μm^2 (Luo, Mohan, Iglesias, & Robinson, 2013; Schiffhauer et al., 2016; Zhang & Robinson, 2005). The accumulation dynamics of proteins to the area of applied stress can be determined by fluorescently tagging a protein of interest and quantifying the ratio of intensity in the pipette to that in other regions of the cell. Two distinct types of deformations are observed in the cortex during MPA. The cortical cytoskeletal network dilates at the tip of the aspirated region, increasing in area. The cortical region along the neck undergoes shear deformation, where the geometry of the network is changing via alterations in the angles of actin filaments to one another. Using a course-grained molecular mechanics model, we have determined that when a cell is aspirated to $L_p = 4R_p$ the increase in area of the tip region of the cell is about twofold, while the network angle change at the neck is about 45 degrees (Luo et al., 2013).

1.4 EXPERIMENTAL SETUP

An epifluorescence microscope, such as the Olympus IX81 with DIC and fluorescence imaging capability, is connected to a motorized water manometer. The manometer is operated through a keypad controller, which allows for the rapid raising or lowering of one of the water tanks to create a height differential (h) between the water tank and the cell. As a result, a precise pressure differential

($\Delta P = \rho g h$, where ρ is the density of water (1 g/cm^3), g is the gravitational coefficient (9.8 m/s^2), and h is the height differential) is applied to the cell through the micropipette. Micropipettes can be purchased (World Precision Instrument, Fire-polished Pre-Pulled Glass Pipettes, TIP5TW1). Alternatively, they may be forged in-house, using thin-wall borosilicate glass tubing (Sutter Instrument, 1 mm outer diameter, 0.75 mm inner diameter, 10 cm length) on a micropipette puller (Micro-Data Instrument, PMP102). We find that micropipettes with a diameter approximately equal to the radius of the cell generally work well for most cell types. The micropipette is spatially controlled on the system by a micromanipulator. For a detailed description of the setup of an MPA system, see Kee & Robinson (2013).

1.4.1 Balancing the system

A micropipette is filled with assay medium and loaded onto the micromanipulator. After locating the micropipette in the field of view at 40× magnification, 1-μm beads are added to an imaging chamber containing the assay medium. With the two water tanks at a level position, the pipette is brought close to the diffusing beads using the micromanipulator. The level of one tank is manually adjusted until no force acts on the beads: they are neither drawn nor pushed away by liquid flow from the micropipette.

1.4.2 Cortical tension (T_c) measurements

Cells in media are placed in an imaging chamber, where the micropipette is then loaded at zero pressure. Pressure is applied to a healthy cell that is entirely in suspension, starting with relatively low pressures (in the 0.1 nN/μm^2 range) and increasing stepwise until the cell is deformed inside the pipette to $L_p = R_p$. The pressure necessary to reach this level of deformation is the critical pressure (P_c), and the cortical tension (T_c) is calculated using Eq. (1). Each cell is measured at least twice to ensure mechanical uniformity for a specific cell. Occasionally the cell membrane will dissociate from the cortex, resulting in rapidly expanding blebs inside the pipette; data for these cells must be discarded.

1.4.3 Quantification for protein mechanoaccumulation

Cells are placed in imaging media such as MES starvation buffer for *Dictyostelium* or Leibowitz L-15 media without phenol red (Invitrogen) for mammalian cells to minimize background fluorescence. Cells are aspirated using a fixed pressure, normally the pressure required by the specific cell type to reach $L_p = 2R_p$. This pressure is reached in the pipette prior to contacting the cell, assuring that the pressure applied is instantaneous and not gradual. The cell is imaged by time-lapse both in DIC and fluorescence channels. The normalized intensity of the protein of interest at the site of stress can be calculated by measuring the mean gray value of the stressed region (I_s), the cortex on the opposite side of the cell from the pipette (I_o), and a background region above or below the cell (I_b), and then using the equation $(I_s - I_b)/(I_o - I_b)$.

2. FLUORESCENCE CORRELATION SPECTROSCOPY

2.1 OVERVIEW

The diffusion and mobility of a protein dictates its lifetime dynamics and the complexes it may be part of. This information is invaluable for developing quantitative models that explain the behavior of the individual protein, and ultimately, the process in which it participates. Macromolecules can passively diffuse or actively move within the cytoplasm of a cell. Passive diffusion is dependent upon the viscosity of the cytoplasm and the size and shape of the molecule, occurring on the order of 5 $\mu m^2/s$. Molecular motors, such as kinesin and myosin, drive-directed transport along microtubules and actin, moving cargo on the order of 1 μm/s. Molecular motors can also "stir" the cytoplasm, actively increasing the apparent diffusion of a protein (Guo et al., 2014). Determining diffusion times of proteins may help decipher mechanisms of a process, and help establish mathematical models that predict biological behavior. Models that describe the mechanosensing behavior of proteins and the cortical viscoelasticity of the cell enhance our understanding of the role of a mechanical meshwork of actin, motors, and cross-linking proteins during furrow ingression (Luo et al., 2013, 2012; Mohan, Luo, Robinson, & Iglesias, 2015; Poirier, Ng, Robinson, & Iglesias, 2012).

Fluorescence correlation spectroscopy (FCS) is a particularly powerful method for measuring diffusion and mobility inside cells. FCS has been used to measure diffusion of molecules in vitro and in vivo, under different stages of the cell cycle and mechanical and pharmacological perturbations. Diffusion and mobility parameters can be extracted from the intensity fluctuations of a fluorescently labeled protein or molecule in a confocal voxel. A correlation function is used to determine the number of fluorescent particles present in the volume over the time course, and single- or multiple-component fits are used to calculate the diffusion time, which is the average time required to diffuse across the confocal volume. The diffusion time extracted is then used to determine diffusion coefficients. This quantitative analysis also provides information on complex assembly and concentration changes. A change in a protein's diffusion time can reflect a change in the cytoskeletal and biochemical interactions in the network. For example, changes in the dynamics of cortexillin I, an actin-bundling protein, and IQGAP2, a scaffolding protein, were studied by FCS in different genetic backgrounds of *Dictyostelium* cells. In an *iqgap2* null background, cortexillin I showed a 30% increase in cytoplasmic diffusion time, suggesting that it engages in different biochemical interactions when IQGAP2 is absent (Srivastava & Robinson, 2015). In addition, FCS was used to demonstrate that global mechanical stresses change protein dynamics, as cortexillin I in compressed cells had twofold slower diffusion rates (Srivastava & Robinson, 2015). The ability to study these dynamics in live cells on the microsecond and nanometer scale is crucial for understanding how changes in the cell cycle and external perturbations affect protein diffusion and mobility, which ultimately affect the cell's biochemistry.

2.2 EXPERIMENTAL SETUP

A laser-scanning confocal microscope, such as the Zeiss 780, can be used with a 40× water objective (typically with a numerical aperture of 1.2) to image a confocal volume of approximately 0.5 fL. An avalanche photodiode detects the fluorescence fluctuations within the volume and the signal is autocorrelated over time (Fig. 2) (Bacia, Kim, & Schwille, 2006; Bulseco & Wolf, 2013). FCS may also be performed with a total internal reflection fluorescence microscope to image membrane proteins, or with a single-plane illumination microscope to image larger three-dimensional samples, such as embryos (Krieger et al., 2015). Having a small number of particles, ideally less than 100, in the volume is essential for accurately identifying small changes. Software, such as Zen, include equations with single- or multiple-component fits to determine correlation values and diffusion times (Carl Zeiss Microimaging, Guide to Basic FCS Experiments). Fluorescence fluctuations are the result of species mobility, as well as various inter- and intramolecular interactions. Fluctuations may also occur due to a change in intrinsic fluorescence, often from a triplet state, in which the fluorophore has transitioned to a dark state. To correct for these fluctuations, a triplet-state component must be added to the model.

Correlating the fluorescence fluctuations over time yields a plot as seen in Fig. 2C. After accounting for the triplet state, the peak correlation amplitude is the autocorrelation value (G_x). The algorithm extracts the particle number ($G_x = 1/N$, where N is the number of particles); a smaller particle number will have a greater autocorrelation value. The diffusion time is extracted from the decay

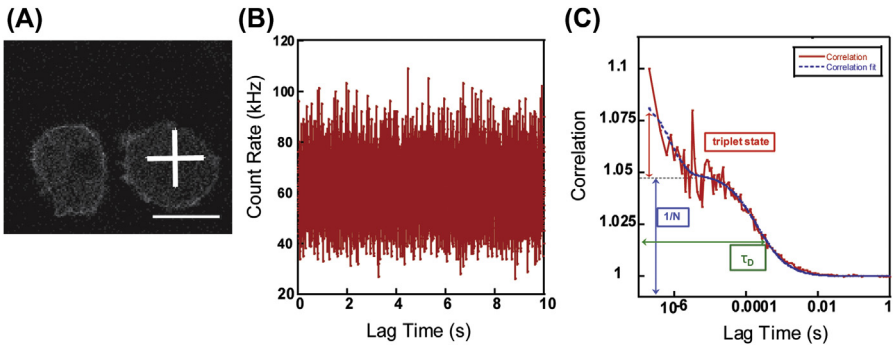

FIGURE 2 Fluorescence Correlation Spectroscopy to assess protein dynamics in live cells: microseconds to milliseconds.

(A) *Dictyostelium* cell expressing GFP-cortexillin I. *Cross* indicates location of the confocal volume. (B) Fluorescence fluctuations recorded over a 10-s time-lapse. (C) Sample autocorrelation plot of fluorescence correlation spectroscopy. *Red (dark gray in print versions) line* represents the autocorrelation data, while the *blue (black in print versions) dashed line* indicates correlation fit based on a one-component model. A triplet-state component has been added. The peak correlation amplitude is proportional to the number of particles, *N*, while the decay of the slope determines the diffusion time, τ_D. Scale, 10 μm.

of the slope, and a diffusion coefficient may be calculated by Eq. (2), the Stokes–Einstein equation:

$$D = \frac{k_B T}{6\pi\eta r} \tag{2}$$

where k_B is the Boltzmann constant, T is temperature, η is the viscosity, and r is the Stokes radius of the particle.

2.2.1 Calibration of the system

Calibrating the system using a fluorescent molecule with a known diffusion coefficient allows for measurement of the size and shape of the confocal volume created by the laser and pinhole. This calibrating fluorophore should fluoresce at the same wavelength as the fluorescently labeled species of interest to accurately define the confocal volume that will be imaged. An example dye is rhodamine 6G, which diffuses at 426 $\mu m^2/s$ and may be used in a water or buffer solution at 50–200 nM (Bacia et al., 2006; Srivastava & Robinson, 2015). The correct focus is found by scanning from the bottom of the cover glass using a reflected laser light, and moving up 200 μm into the sample. The correction collar of the objective must be adjusted to achieve the highest count rate from the dye. This adjustment corrects for the thickness of the cover glass. Next, the pinhole must be aligned; most software have automatic adjustments in the x and y directions to maximize the count rate from the dye. The pinhole should be set to one airy unit to create the smallest confocal volume possible.

2.2.2 Monitoring fluorescence fluctuations

When imaging the calibration dye or a fluorescently labeled species in solution, images can be acquired continuously for 10 seconds with 10 repetitions. When imaging in live cells, shorter acquisition times with fewer repetitions (we typically use five repetitions of 2 second time-lapses for *Dictyostelium*) should be used to avoid artifacts from active cell migration and photobleaching.

2.2.3 Fitting to models

The fluorescence fluctuations over time are analyzed to yield an autocorrelation value, G_x (Eq. (3)):

$$G_x = \frac{\langle \delta F(t) \cdot \delta F(t+\tau) \rangle}{\langle F(t) \rangle^2} \tag{3}$$

where t is time and $F(t)$ is the fluorescence fluctuation detected. While G_x is a value from 0 to 1, 0 being no correlation and 1 being complete correlation, the software adjusts this range from 1 to 2 to simplify calculations (Bulseco & Wolf, 2013).

To determine an accurate diffusion time, a few parameters must be set. The structural parameter is the ratio of the axial resolution to the radial resolution, and is typically between 5 and 7. This is calculated from the diffusion time of the calibration dye. To account for the triplet-state excitation, a triplet-state component is added to

the fit. However, since this state should be rapid, its fit should be restricted to a maximum of 8 μs. In addition, the data can be fit to a single-component or multiple-component 3D diffusion model, depending on the species measured. Because the algorithm may not correctly identify separate groups within the data, we often prefer to focus on simpler models that include single components. The data are then fit to a one-component model to generate a parameter set that may represent a distribution of species.

2.2.4 Data analysis

Once the correlation plots have been fit to the models, the resulting parameters can be analyzed to extract information on the number of species within the volume and their average diffusion time. However, not every trace may fit the model well. The residual trace shows how the data deviate from the fit and is helpful in determining whether the model is an accurate representation of the data. Occasionally the fluorescently labeled species may aggregate, either in solution or in live cells. During live cell FCS, an organelle or large fluorescing species may enter the imaging volume. Such aggregates or disturbances can be detected in the trace as significant deviations or nonuniform fluctuations in the count rate. These traces may be removed from the analysis. Traces that show photobleaching over time should also be discarded. The remaining traces are averaged, the data are fit to the model, and an average diffusion time is extracted. This diffusion time can then be converted into a diffusion coefficient using the dye as calibration for the confocal volume shape and size (Carl Zeiss Microimaging, Guide to Basic FCS Experiments). This analysis is used to measure diffusion times, and also to determine the assembly of complexes, binding stoichiometry, and changes in the network. To measure interactions between two specific proteins or molecules, FCS may be performed with two colors, a technique known as fluorescence cross-correlation spectroscopy (FCCS) (see Section 2.2.4.1).

3. FLUORESCENCE CROSS-CORRELATION SPECTROSCOPY

FCCS involves imaging intensity fluctuations of two different fluorophores within the same focal volume. A significant cross-correlation between the species suggests that the two species might associate based on the probability of the two different fluorophores diffusing in or out of the volume simultaneously. FCCS allows for quantitative interaction measurements between two species in vitro and detection of associative interactions in vivo, yielding information on interaction strengths, dissociation constants, and binding stoichiometries. Traditional methods of studying protein−protein interactions in cells, such as coimmunoprecipitation (co-IP) and Förster resonance energy transfer (FRET), have their own significant limitations. Co-IP requires lysing the cells and a time delay as the extracts are exposed to beads, washed, and eluted; this readily detects very stable associations, but disrupts more transient ones. FRET requires that the donor and acceptor fluorophores reside within a minimal distance in a relatively optimal orientation. FCCS circumvents both types

of issues; cells remain intact, and fluorophores do not have to reside within an optimal distance or orientation. Performing FCCS in vivo facilitates analysis of protein–protein interactions in context and allows for the relatively easy process of incorporating acute and genetic perturbations. In the context of cytokinesis, it allows for a comparison between interactions at the cleavage furrow and those that occur globally. In addition, FCCS is sensitive enough to identify transient interactions that may not be detectable by co-IP (Bacia et al., 2006; Bacia & Schwille, 2007).

FCCS requires that two species be labeled with different fluorophores with little overlap in excitation and emission spectra to prevent cross-talk. However, the confocal volumes must have significant overlap to allow for accurate cross-correlation. If the system has one confocal pinhole, then the volume must be adjusted to a single wavelength. However, if two pinholes are used, the two volumes may be set for closer overlap. Although FCCS in vitro can provide reliable measurement of a dissociation constant, K_d, measurement in vivo is limited to relative interaction strengths. This limitation comes from the fact that proteins may be involved in interactions with multiple cellular factors, which complicates the measurement of a true K_d. Further, expression of the fluorescent protein in addition to an unlabeled endogenous population complicates the K_d assessment as well. In addition, the presence of organelles and cytoskeletal networks will also affect cross-correlation. However, the relative interaction strength is still a valuable measurement for characterizing novel, transient interactions that have an impact on biological processes.

The cross-correlation function, G_x, is a measure of how well the fluorescence fluctuations from the two different channels correlate over time, and is calculated using Eq. (4):

$$G_x = \frac{\langle \delta F_A(t) \cdot \delta F_B(t+\tau) \rangle}{\langle F_A(t) \rangle \langle F_B(t) \rangle} \tag{4}$$

where t is time, and $F(t)$ is the fluorescence fluctuation in either the green or red channel. The cross-correlation value ranges from 0 to 1, with 0 being no cross-correlation, and 1 being complete correlation. The scale is again adjusted from 1 to 2, and we find that values generally range between 1.001 and 1.1 in live cells, and between 1.05 and 1.2 for species in solution.

The experimental setup used for FCCS is similar to the one used for FCS, but the additional laser that excites the second fluorophore creates a second confocal volume. When acquiring traces, the two lasers simultaneously excite the sample, and fluorescence fluctuations from both channels are recorded. This results in three plots: two autocorrelation plots (one for each channel), and one cross-correlation plot. The traces with aggregates or photobleaching are discarded, and the correlations are fit to the model. A relative interaction strength (IS^{-1}) may be calculated with Eq. (5):

$$IS^{-1} = \frac{G_x}{V_{eff} G_A G_B} \left(\frac{G_A}{G_x} - 1 \right) \left(\frac{G_B}{G_x} - 1 \right) \tag{5}$$

where V_{eff} is the effective overlap between the confocal volumes (set to 1), G_A and G_B are the individual channel correlation values, and G_x is the cross-correlation

value (Bierbaum & Bastiaens, 2013). This equation takes the form of a dissociation constant by comparing the fraction of bound molecules (from G_x) to the free molecules. The values are normalized against the autocorrelations of G_A and G_B.

While FCCS yields information about relative interaction strengths, understanding the dynamic range of the setup is critical. Two fluorescently labeled proteins that are known to bind or two fluorescent proteins linked by a short amino acid sequence may be used as positive controls. As a negative control, two unlinked fluorescent proteins may be used to reveal the dynamic range, which we find is ~10-fold. FCCS is becoming an increasingly valuable technique to directly measure protein–protein interactions in vivo and will continue to allow for the study of transient interactions.

4. FLUORESCENCE RECOVERY AFTER PHOTOBLEACHING

4.1 OVERVIEW

Fluorescence recovery after photobleaching (FRAP) is a commonly used technique to measure turnover dynamics of proteins in cells. A region of a cell expressing the fluorescent protein of interest is photobleached using a laser, and that region is imaged over time to measure the rate of fluorescence recovery by unbleached, fluorescent molecules from outside the region (Jacobson, Derzko, Wu, Hou, & Poste, 1976; Lippincott-Schwartz, Snapp, & Kenworthy, 2001). The resulting recovery curve can be used to calculate the rate of movement, the release time from other binding interactions, and the fraction of the protein that is mobile. For proteins that recover on the order of hundreds of milliseconds to seconds, the recovery time is generally dominated by the unbinding kinetics of the protein from its binding partners. This unbinding may reflect the release time of the bleached protein or, more commonly, release of the unbleached protein from nearby pools. In contrast, a protein with low turnover dynamics may be incredibly stable. Proteins may also fail to recover to the initial fluorescence intensity due to their deep associations in larger complexes and networks. Once the images have been corrected for photobleaching, the percentage recovery represents the population of the protein that is mobile within the cell.

We have shown that during cytokinesis, equatorially enriched proteins, including myosin II, cortexillin I, and IQGAP2, are stabilized under increasing mechanical stress. Cells under compression by agarose overlay demonstrate an increase in the immobile fraction in interphase cells and at the cleavage furrow of dividing *Dictyostelium* cells. The increase in mechanical load stabilizes the cytoskeletal meshwork, therefore increasing the immobile fraction of these proteins. In *myosin II* null cells, cortexillin I and IQGAP2 immobile fractions also increase, although their diffusion times do not. Thus, myosin II promotes distinct cytoskeletal network properties, reflected in these protein mobility differences (Srivastava & Robinson, 2015). Similar increases in the immobile fraction of myosin II have been observed in mammalian cytokinesis as well (Kondo et al., 2011).

With FRAP, one can assess protein dynamics of different regions of the cell, including the cortex and cytoplasm. Imaging these dynamics on the hundreds of milliseconds to seconds timescales with micrometer resolution provides insight into more global changes during cytokinesis, and can reveal alterations in networks and stabilities of complexes.

4.2 EXPERIMENTAL SETUP

A few images of the region of interest are taken to quantify the intensity of the fluorescence before photobleaching. A small region is photobleached with a laser of the excitation wavelength of the fluorescent protein. This region is then imaged over time until recovery has saturated. An unbleached region of the cell is also imaged simultaneously to account for photobleaching due to image acquisition over time. The average intensity of the bleached region, the control unbleached region, and background are quantified (Fig. 3).

After background correction, the intensity is fit to a single exponential form, Eq. (6):

$$\mathrm{NI}(t) = m_1\left(1 - m_2 \cdot \mathrm{e}^{-kt}\right) \tag{6}$$

where m_1 and m_2 are fitting parameters. The immobile fraction may be quantified by Eq. (7):

$$F_\mathrm{i} = \frac{1 - m_1}{1 - m_1 + m_2} \tag{7}$$

Quantifying this recovery of intensity can yield insight into the kinetics and complexes of protein dynamics (Srivastava & Robinson, 2015).

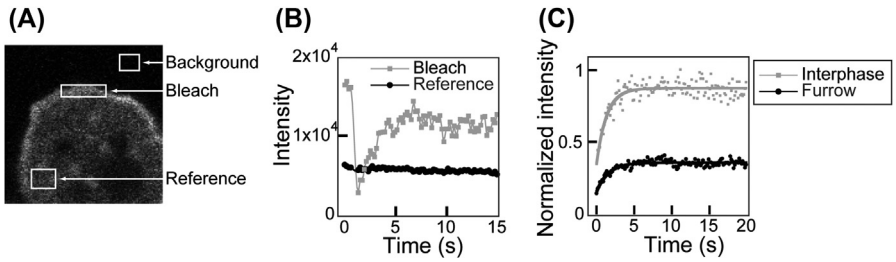

FIGURE 3 Fluorescence Recovery after Photobleaching to determine protein mobility and recovery: milliseconds to seconds.

(A) A sample image of GFP-cortexillin I expressed in *Dictyostelium*, demonstrating the bleach site. (B) Sample fluorescence intensity curves. (C) After background subtraction, the reference intensity remains constant, while the bleached region shows a stereotypical decrease and recovery of fluorescence over time.

Adapted from Srivastava, V. & Robinson, D. N. (2015). Mechanical stress and network structure drive protein dynamics during cytokinesis. Current Biology, 25, *663–670.*

CONCLUSION

MPA, FCS, and FRAP are currently used to measure the biochemical and mechanical aspects of cytokinesis on the time- and length-scales of mechanoresponses, mobility, protein interactions, and network dynamics in live cells. Other techniques, including optical traps and single-molecule imaging, are contributing to our understanding of protein dynamics as well (Ren et al., 2009; Spudich, Rice, Rock, Purcell, & Warrick, 2011). In addition, the introduction of chemically inducible dimerization systems, optogenetics, lattice-light sheet microscopy, and other superresolution microscopy will bring exciting, new quantitative measurements to the field (Chen et al., 2014; Laplant, Huang, Bewersdorf, & Pollard, 2016; Strickland et al., 2012). These techniques can be combined with the tools of genetics, pharmacological agents, and global compression to allow for a rich dissection of individual components involved (Kee et al., 2012; Srivastava & Robinson, 2015). The benefit of these live-cell techniques is the ability to observe and make quantitative measurements of cell mechanics and protein dynamics as the cell undergoes important physiological processes. These mechanics and protein dynamics measurements, especially when combined with other metrics of cell morphological changes, such as furrow ingression kinetics, yield mechanistic insight into pathways and molecular interactions and can even lead to molecular models that predict cellular behaviors (Luo et al., 2012; Mohan et al., 2015; Poirier et al., 2012; Zhang & Robinson, 2005; Zhou et al., 2010). This collection of methods will continue to provide fascinating insight into the mechanical and biochemical mechanisms of cytokinesis.

ACKNOWLEDGMENTS

This work is supported by the National Institutes of Health grants GM66817 and GM109863 to D.N.R. We thank members of the Robinson lab and Vasudha Srivastava for their valuable comments during manuscript preparation.

REFERENCES

Ashkin, A., Dzeidzic, J. M., & Yamane, T. (1987). Optical trapping and manipulation of single cells using infrared laser beams. *Nature, 330*, 769–771.

Bacia, K., Kim, S. A., & Schwille, P. (2006). Fluorescence cross-correlation spectroscopy in living cells. *Nature Methods, 3*, 83–89.

Bacia, K., & Schwille, P. (2007). Practical guidelines for dual-color fluorescence cross-correlation spectroscopy. *Nature Protocols, 2*, 2842–2856.

Bierbaum, M., & Bastiaens, P. H. (2013). Cell cycle-dependent binding modes of the ran exchange factor RCC1 to chromatin. *Biophysical Journal, 104*, 1642–1651.

Bulseco, D. A., & Wolf, D. E. (2013). Chapter 21 – fluorescence correlation spectroscopy: molecular complexing in solution and in live cells. *Methods in Cell Biology, 114*, 489–524.

Carl Zeiss Microimaging, Inc. Guide to basic FCS experiments on Zeiss LSM 780/Confocor 3/BiG systems running ZEN 2010.

Chen, B. C., Legant, W. R., Wang, K., Shao, L., Milkie, D. E., Davidson, M. W., … Betzig, E. (2014). Lattice light-sheet microscopy: imaging molecules to embryos at high spatiotemporal resolution. *Science, 346*, 1257998.

Crick, F. H. C., & Hughes, A. F. W. (1950). The physical properties of cytoplasm. *Experimental Cell Research, 1*, 37−80.

Effler, J. C., Iglesias, P. A., & Robinson, D. N. (2007). A mechanosensory system controls cell shape changes during mitosis. *Cell Cycle, 6*, 30−35.

Gerald, N., Dai, J., Ting-Beall, H. P., & De Lozanne, A. (1998). A role for *Dictyostelium* racE in cortical tension and cleavage furrow progression. *The Journal of Cell Biology, 2*, 483−492.

Guo, M., Ehrlicher, A. J., Jensen, M. H., Renz, M., Moore, J. R., Goldman, R. D., … Weitz, D. A. (2014). Probing the stochastic, motor-driven properties of the cytoplasm using force spectrum microscopy. *Cell, 4*, 822−832.

Hiramoto, Y. (1963). Mechanical properties of sea urchin eggs. II. Changes in mechanical properties from fertilization to cleavage. *Experimental Cell Research*, 76−89.

Hiramoto, Y. (1990). Mechanical properties of the cortex before and during cleavage. *Annals of the New York Academy of Sciences, 582*, 22−30.

Hochmuth, R. M. (2000). Micropipette aspiration of living cells. *Journal of Biomechanics, 1*, 15−22.

Jacobson, K., Derzko, Z., Wu, E.-S., Hou, Y., & Poste, G. (1976). Measurement of the lateral mobility of cell surface components in single, living cells by fluorescence recovery after photobleaching. *Journal of Supramolecular Structure, 5*, 565−576.

Kee, Y.-S., Ren, Y., Dorfman, D., Iijima, M., Firtel, R., Iglesias, P. A., & Robinson, D. N. (2012). A mechanosensory system governs myosin II accumulation in dividing cells. *Molecular Biology of the Cell, 23*, 1510−1523.

Kee, Y.-S., & Robinson, D. N. (2013). Micropipette aspiration for studying cellular mechanosensory responses and mechanics. *Methods in Molecular Biology, 983*, 367−382.

Kim, J. H., Ren, Y., Ng, W. P., Li, S., Son, S., Kee, Y.-S., … Chen, E. H. (2015). Mechanical tension drives cell membrane fusion. *Developmental Cell, 32*, 561−573.

Kondo, T., Hamao, K., Kamijo, K., Kimura, H., Morita, M., Takahashi, M., & Hosoya, H. (2011). Enhancement of myosin II/actin turnover at the contractile ring induces slower furrowing in dividing HeLa cells. *Biochemical Journal, 435*, 569−576.

Krieger, J. W., Singh, A. P., Bag, N., Garbe, C. S., Saunders, T. E., Langowski, J., & Wohland, T. (2015). Imaging fluorescence (cross-) correlation spectroscopy in live cells and organisms. *Nature Protocols, 10*, 1948−1974.

Laplant, C., Huang, F., Bewersdorf, J., & Pollard, T. D. (2016). High-speed super-resolution imaging of live fission yeast cells. J.M. Walker (Series Ed.). In A. Sanchez-Diaz, & P. Perez (Eds.), *Methods in molecular biology: Yeast cytokinesis, methods and protocols* (pp. 45−57). New York: Humana Press.

Lippincott-Schwartz, J., Snapp, E., & Kenworthy, A. (2001). Studying protein dynamics in living cells. *Nature Reviews Molecular Cell Biology, 2*, 445−456.

Luo, T., Mohan, K., Iglesias, P. A., & Robinson, D. N. (2013). Molecular mechanisms of cellular mechanosensing. *Nature Materials, 11*, 1064−1071.

Luo, T., Mohan, K., Srivastava, V., Ren, Y., Iglesias, P. A., & Robinson, D. N. (2012). Understanding the cooperative interaction between myosin II and actin cross-linkers mediated by actin filaments during mechanosensation. *Biophysical Journal, 2*, 238−247.

Luo, T., Srivastava, V., Ren, Y., & Robinson, D. N. (2014). Mimicking the mechanical properties of the cell cortex by the self-assembly of an actin cortex in vesicles. *Applied Physics Letters, 15*, 153701.

Matzke, R., Jacobson, K., & Radmacher, M. (2001). Direct, high-resolution measurement of furrow stiffening during division of adherent cells. *Nature Cell Biology, 3*, 607–610.

Mijailovich, S. M., Kojic, M., Zivkovic, M., Fabry, B., & Fredberg, J. J. (2002). A finite element model of cell deformation during magnetic bead twisting. *Journal of Applied Physiology, 93*, 1429–1436.

Mohan, K., Luo, T., Robinson, D. N., & Iglesias, P. A. (2015). Cell shape regulation through mechanosensory feedback control. *Journal of the Royal Society Interface, 12*, 201501512.

Otto, O., Rosendahl, P., Mietke, A., Golfier, S., Herold, C., Klaue, D., … Guck, J. (2015). Real-time deformability cytometry: on-the-fly cell mechanical phenotyping. *Nature Methods, 12*, 199–202.

Poirier, C. C., Ng, W. P., Robinson, D. N., & Iglesias, P. A. (2012). Deconvolution of the cellular force-generating subsystems that govern cytokinesis furrow ingression. *PLoS Computational Biology, 8*(4), e1002467.

Rappaport, R. (1967). Cell division: direct measurement of maximum tension exerted by furrow of echinoderm eggs. *Science, 156*, 1241–1243.

Reichl, E. M., Ren, Y.-S., Morphew, M. K., Delannoy, M., Effler, J. C., Girard, K. D., … Robinson, D. N. (2008). Interactions between myosin and actin crosslinkers control cytokinesis contractility dynamics and mechanics. *Current Biology, 7*, 471–480.

Ren, Y.-S., Effler, J. C., Norstrom, M., Luo, T., Firtel, R. A., Iglesias, P. A., … Robinson, D. N. (2009). Mechanosensing through cooperative interactions between myosin II and the actin crosslinker cortexillin I. *Current Biology, 19*, 1421–1428.

Schiffhauer, E. S., Luo, T., Mohan, K., Srivastava, V., Qian, X., Griffis, E. R., … Robinson, D. N. (2016). Mechanoaccumulative elements of the mammalian actin cytoskeleton. *Current Biology* (in press).

Spudich, J. A., Rice, S. E., Rock, R. S., Purcell, T. J., & Warrick, H. M. (2011). The optical trapping dumbbell assay for nonprocessive motors or motors that turn around filaments. *Cold Spring Harbor Protocols, 11*, 1372–1374.

Srivastava, V., Iglesias, P. A., & Robinson, D. N. (2015). Cytokinesis: robust cell shape regulation. *Seminars in Cell & Developmental Biology* (in press).

Srivastava, V., & Robinson, D. N. (2015). Mechanical stress and network structure drive protein dynamics during cytokinesis. *Current Biology, 25*, 663–670.

Strickland, D., Lin, Y., Wagner, E., Hope, C. M., Zayner, J., Antoniou, C., … Glotzer, M. (2012). TULIPs: tunable, light-controlled interacting protein tags for cell biology. *Nature Methods, 9*, 379–384.

Sun, Q., Luo, T., Ren, Y., Florey, O., Shirasawa, S., Sasazuki, T., … Overholtzer, M. (2014). Competition between human cells by entosis. *Cell Research, 24*, 1299–1310.

Wolpert, L. (1966). The mechanical properties of the membrane of the sea urchin egg during cleavage. *Experimental Cell Research, 2*, 385–396.

Yang, L., Effler, J. C., Kutscher, B. L., Sullivan, S. P., Robinson, D. N., & Iglesias, P. A. (2008). Modeling cellular deformations using the level set formalism. *Biomedcentral Systems Biology, 2*, 68–84.

Zhang, W., & Robinson, D. N. (2005). Balance of actively generated contractile and resistive forces controls cytokinesis dynamics. *Proceedings of the National Academy of Sciences of the United States of America, 20*, 7186–7191.

Zhou, Q., Kee, Y.-S., Poirier, C. C., Jelinek, C., Osborne, J., Divi, S., … Robinson, D. N. (2010). 14-3-3 coordinates microtubules, Rac, and myosin II to control cell mechanics and cytokinesis. *Current Biology, 20*, 1881–1889.